MR Molecular Imaging of Aortic Angiogenesis

Kejia Cai, PHD, Shelton D. Caruthers, PHD, Wenjing Huang, BS, Todd A. Williams, RT,
Huiying Zhang, MD, Samuel A. Wickline, MD, Gregory M. Lanza, MD, PHD,
Patrick M. Winter, PHD

St. Louis, Missouri

OBJECTIVES The objectives of this study were to use magnetic resonance (MR) molecular imaging to 1) characterize the aortic neovascular development in a rat model of atherosclerosis and 2) monitor the effects of an appetite suppressant on vascular angiogenesis progression.

BACKGROUND The James C. Russell:LA corpulent rat strain (JCR:LA-cp) is a model of metabolic syndrome characterized by obesity, insulin resistance, hyperlipidemia, and vasculopathy, although plaque neovascularity has not been reported in this strain. MR molecular imaging with $\alpha_v\beta_3$-targeted nanoparticles can serially map angiogenesis in the aortic wall and monitor the progression of atherosclerosis.

METHODS Six-week old JCR:LA-cp (+/?; lean, n = 5) and JCR:LA-cp (cp/cp; obese, n = 5) rats received standard chow, and 6 obese rats were fed the appetite suppressant benfluorex over 16 weeks. Body weight and food consumption were recorded at baseline and weeks 4, 8, 12, and 16. MR molecular imaging with $\alpha_v\beta_3$-targeted paramagnetic nanoparticles was performed at weeks 0, 8, and 16. Fasted plasma triglyceride, cholesterol, and glucose were measured immediately before MR scans. Plasma insulin and leptin levels were assayed at weeks 8 and 16.

RESULTS Benfluorex reduced food consumption (p < 0.05) to the same rate as lean animals, but had no effect on serum cholesterol or triglyceride levels. MR (3-T) aortic signal enhancement with $\alpha_v\beta_3$-targeted nanoparticles was initially equivalent between groups, but increased (p < 0.05) in the untreated obese animals over 16 weeks. No signal change (p > 0.05) was observed in the benfluorex-treated or lean rat groups. MR differences paralleled adventitial microvessel counts, which increased (p < 0.05) among the obese rats and were equivalently low in the lean and benfluorex-treated animals (p > 0.05). Body weight, insulin, and leptin were decreased (p < 0.05) from the untreated obese animals by benfluorex, but not to the lean control levels (p < 0.05).

CONCLUSIONS Neovascular expansion is a prominent feature of the JCR:LA-cp model. MR imaging with $\alpha_v\beta_3$-targeted nanoparticles provided a noninvasive assessment of angiogenesis in untreated obese rats, which was suppressed by benfluorex. (J Am Coll Cardiol Img 2010;3:824–32) © 2010 by the American College of Cardiology Foundation

The prevalence of obesity, metabolic syndrome, and diabetes is rapidly increasing in Western populations along with their secondary complications, particularly cardiovascular disease. Unfortunately, the acceleration of atherosclerosis is generally silent and difficult to monitor until the manifestations become symptomatic. Serum biomarkers, such as low-density lipoprotein or high-sensitivity C-reactive protein, offer nonspecific but possibly predictive indications of cardiovascular risk, but neither specifically quantifies the temporospatial microscopic and biochemical changes occurring in the atherosclerotic vessel wall (1–3). As an alternative to monitoring systemic indexes, molecular imaging may allow noninvasive assessment of disease biomarkers directly within the involved tissues. For example, plaque angiogenesis is correlated with plaque rupture and often occurs alongside other morphological features of vulnerable lesions including macrophage infiltration, lipid-rich cores, and thin-cap shoulders (4–8). Therefore, plaque neovasculature could be indicative of intramural atherosclerotic severity and overall cardiovascular disease risk.

Our laboratory developed an $\alpha_v\beta_3$-targeted paramagnetic nanoparticle agent ($\sim$250 nm diameter) for noninvasive molecular imaging of angiogenesis in animal models of cancer and cardiovascular disease as well as for monitoring response to targeted antiangiogenic therapy (9–12). The overall aim of this study was to use $\alpha_v\beta_3$-integrin paramagnetic nanoparticles for monitoring the temporal progression of aortic angiogenesis in a rat model of metabolic syndrome and for evaluating the effects of a known cardioprotective therapy, benfluorex, on adventitial neovascularization.

The James C. Russell:LA corpulent rat strain (JCR:LA-cp) is a unique model of metabolic syndrome characterized by spontaneous atherosclerosis and ischemic myocardial lesions due to obesity, hyperlipidemia, and insulin resistance (13–16). This disease model arises from a genetic mutation in the leptin receptor, commonly referred to as the corpulent gene (cp) (15). Animals that are homozygous for the cp gene are denoted as JCR:LA-cp cp/cp obese, whereas animals that are heterozygous (cp/+) or homozygous for the functional leptin receptor gene (+/+) are indistinguishable and denoted as JCR:LA-cp +/? lean. The obese animals display a phenotype consistent with metabolic syndrome and the lean animals serve as normal controls. The prevalence of plaque angiogenesis as a

vascular biomarker of atherosclerosis in metabolic syndrome is poorly understood and undocumented in the JCR:LA-cp rat model. Previous studies demonstrated that benfluorex, an anorectic and hypolipidemic drug, decreases insulin resistance, normalizes the lipid profile, and diminishes aortic plaque in JCR:LA-cp rats (17–19).

METHODS

Experimental design. Six-week old male JCR:LA-cp (+/?, lean rats, n = 5) and JCR:LA-cp (cp/cp, obese rats, n = 11) were studied. Six obese rats received dietary benfluorex (Sigma-Aldrich, St. Louis, Missouri) ad libitum (0.069% wt/wt; Purina Mills, St. Louis, Missouri) for 16 weeks, and the remaining obese (n = 5) and lean (n = 5) rats were fed a standard rodent diet (Purina Mills). Body weight and food consumption were recorded at baseline and weeks 4, 8, 12, and 16 of the study. Magnetic resonance (MR) molecular imaging with $\alpha_v\beta_3$-targeted paramagnetic nanoparticles (1.0 ml/kg, $\sim$0.005 mmol Gd^{3+}/kg, $\sim$200 pmol nanoparticles/kg) was performed at baseline and at weeks 8 and 16. The study protocol was approved by the Animal Studies Committee of Washington University Medical School.

Nanoparticle formulation. The nanoparticle contrast agent was prepared for MR experiments as described in previous reports (9–12). Nanoparticle emulsions were composed of perfluorocarbon (20%, vol/vol) and excipient (80%, vol/vol). Each nanoparticle contained 98.0% perfluorooctyl bromide (Minnesota Manufacturing and Mining, St. Paul, Minnesota) with 2.0% (wt/vol) of a lipid surfactant comixture in a 1.7% (wt/vol) glycerin in water excipient. The surfactant comixture included 68 mole% lecithin (Avanti Polar Lipids, Inc., Alabaster, Alabama), 0.1 mole% peptidomimetic $\alpha_v\beta_3$-integrin antagonist conjugated to polyethylene glycol (molecular weight of 2,000) phosphatidylethanolamine (Avanti Polar Lipids, Inc.), 1.9 mole% phosphatidylethanolamine (Avanti Polar Lipids, Inc.), and 30 mole% gadolinium diethylenetriamine-pentaacetic acid-bis-oleate (IQsynthesis, St. Louis, Missouri).

Homing to angiogenic vessels was achieved with an $\alpha_v\beta_3$-integrin antagonist, originally developed for nuclear and optical imaging (20,21). The specificity of the $\alpha_v\beta_3$-ligand mirrored that of LM609 as assessed by staining and flow cytometry and had a 15-fold preference for the Mn^{2+} activated recep-

tor (21 nmol/l) (21). The half maximal inhibitory concentration for $\alpha_v\beta_5$, $\alpha_5\beta_1$ and glycoprotein IIb/IIIa was determined to be >10 μM. Integrin-targeted nanoparticles presented approximately 300 ligands per particle with a half maximal inhibitory concentration of 50 pM for the Mn^{2+} activated $\alpha_v\beta_3$-integrin (12).

MR imaging. MR molecular imaging of rat abdominal aorta was conducted under anesthesia (1% to 2% isoflurane in 2 l/min oxygen) using a 3.0-T clinical magnet (Achieva; Philips Healthcare, Andover, Massachusetts); an 11-cm, 2-element phased array coil; and a T1-weighted, fat-suppressed, black-blood, multislice turbo spin echo imaging sequence (TR/TE = 296/10 ms, resolution = 213 μm × 213 μm × 2 mm, 4 slices, ~11.6 min). Four contiguous slices were positioned immediately superior to the renal arteries, which provided an anatomical landmark for reproducible MR slice alignment over the course of the study. Saturation bands were placed proximal and distal to the region of image acquisition to null the blood signal, and fat suppression was achieved with spectral selection attenuated inversion recovery. MR images were acquired before and 120 min after tail vein injection of $\alpha_v\beta_3$-targeted paramagnetic nanoparticles at weeks 0 and 8. At week 16, aortic images were acquired before nanoparticle injection and dynamically at 20, 60, and 120 min post-treatment. All aortic images were normalized to a reference gadolinium standard placed within the field of view. In each transaxial image, the aortic wall was manually traced and the average signal intensity across all slices in each animal was calculated for each time point. MR signal enhancement on each day of the study was calculated for each animal relative to the aortic signal intensity before $\alpha_v\beta_3$-targeted paramagnetic nanoparticle injection.

Clinical and histopathology. At weeks 0, 8, and 16 of the study, blood samples were obtained and analyzed for fasted plasma triglyceride, cholesterol, and glucose using routine clinical chemistry procedures by the Washington University Department of Comparative Medicine. Plasma insulin and leptin levels were assayed by Millipore Bioscience Division (St. Charles, Missouri) at weeks 8 and 16.

After the last imaging time point, abdominal aortas were resected for histology. Formalin-fixed and paraffin-embedded (5 μm) sections were stained for von Willebrand factor, an endothelial cell marker (Chemicon International, Inc., Temecula, California). Four equally spaced histological sections within the imaged segment were exam-

ined for each animal. For each digitized section, adventitial microvessels, consisting of no more than 3 endothelial cells in circumference, were counted and divided by the adventitial area, which was traced and calculated with MATLAB 7.0 (The MathWorks, Inc., Natick, Massachusetts) to estimate microvessel density. Microvessel density (vessels/100 μm^2) was averaged across the 4 microscopic sections to provide a single estimate for each rat.

Statistics. All quantitative data are reported as mean ± SE. Two-way analysis of variance was performed to compare the experimental groups and the repeated measures (SAS Institute, Cary, North Carolina). For significant F tests ($p < 0.05$), group means were separated using the least significant difference technique.

RESULTS

Body weight and food consumption. At baseline, body weight and food consumption in the 6-week-old obese rat groups were 46.5% and 49.2% higher, respectively, than the lean animals (Fig. 1). During the 16 weeks of the study, all treatment groups increased body weight and food consumption. The appetite suppression effect of benfluorex resulted in decreased ($p < 0.05$) weekly food consumption by obese rats relative to the untreated corpulent animals that was similar ($p > 0.05$) to the lean control intake. Although obese rats receiving benfluorex weighed less (517 ± 9 g, $p < 0.05$) than the untreated obese control animals (615 ± 18 g) at 16 weeks, these animals were heavier ($p < 0.05$) than the lean control rats (367 ± 18 g) despite equivalent dietary intakes. From the average daily food consumption, the amount of benfluorex incorporated into the feed and the average weights of the animals, the average drug dose over the course of this study was calculated as 31.8 ± 0.5 mg/kg/day.

MR imaging. The fat suppressed MR images of the heavier obese rats, both benfluorex-treated and untreated, revealed large, hypointense, periaortic adipose regions within the abdominal cavity that were not observed in lean animals (Fig. 2). At 8 and 16 weeks of the study, marked neovascular signal enhancement was measured throughout the aortic slices of the untreated obese rats in contradistinction to the sparse background contrast level detected in the lean animals at 2 h post-injection. Benfluorex treatment reduced the extent and intensity of neovascular signal enhancement observed in the aortic wall of obese rats to a magnitude similar

to that found in the lean animals, which paralleled the primary drug effect on feed consumption (Fig. 3). Dynamic images obtained over 120 min after injection of $\alpha_\nu\beta_3$-targeted paramagnetic nanoparticles at week 16 clearly revealed a marked increase in neovascular contrast at 20 min for the untreated obese rats, whereas signal enhancement in both the lean and benfluorex-treated obese rats was much lower. These differences in contrast enhancement remained unchanged over the remaining time of scanning (Fig. 4).

Clinical pathology. Fasting plasma glucose did not differ among the 3 treatment groups over the course of the study (Fig. 5). As expected, cholesterol and triglyceride concentrations were lower ($p < 0.05$) in lean rats compared with the obese animals, but benfluorex treatment did not decrease ($p > 0.05$) plasma lipids significantly in the obese rats (Fig. 5). Fasting hormonal concentrations of insulin and leptin were markedly higher ($p < 0.05$) in the obese versus lean animals at 8 and 16 weeks (Fig. 5), similar to plasma lipid levels. However, benfluorex lowered ($p < 0.05$) insulin and leptin levels in the obese rats, but not to the level in lean animals.

Histology. Routine light microscopy of the aortas from obese rats showed increased adventitial adipose deposits compared with the lean animals, which paralleled the MR imaging results (Fig. 6). No protruding aortic plaque was appreciated in the obese animals at 22 weeks of age, but subintimal plaque thickening was prevalent in the untreated obese rats and rarely appreciated in the lean control or obese rats fed benfluorex.

Anti–von Willebrand factor staining of endothelial cells revealed a greatly expanded vasa vasorum within the fatty adventitia of the abdominal aorta in untreated obese rats relative to the lean animals. The benfluorex-treated animals displayed only patchy areas of neovascular expansion within the adventitia, involving much less of the vessel wall compared with the untreated obese animals. Adventitial microvessel density in the untreated obese rats (5 ± 0.7 vessel/100 μm^2) was greatly increased ($p < 0.05$) relative to benfluorex-treated obese rats (2.6 ± 0.3 vessel/100 μm^2) and the lean control groups (2.7 ± 0.4 vessel/100 μm^2), which were equivalent (Fig. 7).

DISCUSSION

Metabolic syndrome is characterized by a clustering of metabolic abnormalities in conjunction with underlying insulin resistance and is closely associ-
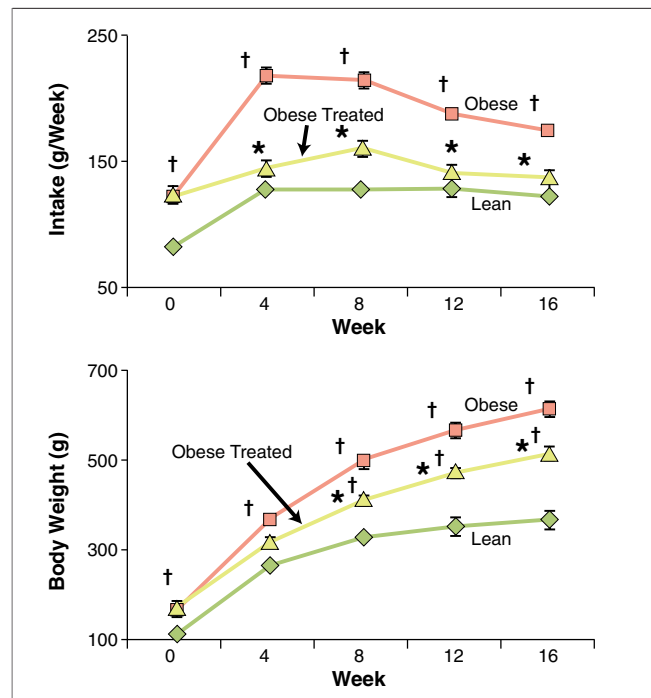

Figure 1. Diet Consumption and Body Weight

Diet consumption (**top**) and body weight (**bottom**) in lean (**green**), obese (**pink**), and obese treated (**yellow**) animals. Benfluorex reduced food consumption and body weight of treated obese rats compared with untreated obese animals. Benfluorex-treated rats were heavier than the lean control animals despite equivalent food intake. *$p < 0.05$ versus untreated obese animals, †$p < 0.05$ versus lean animals.

ated with the onset of diabetes and accelerated cardiovascular disease. The corpulent JCR:LA-cp rat model of metabolic syndrome exhibited obesity, severe insulin resistance, hyperinsulinemia, and hypertriglyceridemia, as reported by others (13–16). Vasa vasorum expansion and neovasculature proliferation, previously unreported in this model, was demonstrated and longitudinally assessed with MR molecular imaging at 3.0-T with $\alpha_\nu\beta_3$-targeted paramagnetic nanoparticles, whereas benfluorex-treated and lean rats had significantly lower MR signal enhancement throughout the study. The MR enhancement observed in the aortic wall of the lean animals was perhaps a result of circulating nanoparticles. In an atherosclerotic rabbit model, the MR enhancement in the aortic wall persisted up to 8 and 12 h for nontargeted and $\alpha_\nu\beta_3$-targeted nanoparticle formulations, respectively (22). Noninvasive MR molecular imaging results were closely corroborated by microscopic estimates of microvessel density within the aortic wall. Both MR and histology objectively measured overall neovascularity by encompassing all regions of the abdominal aorta,
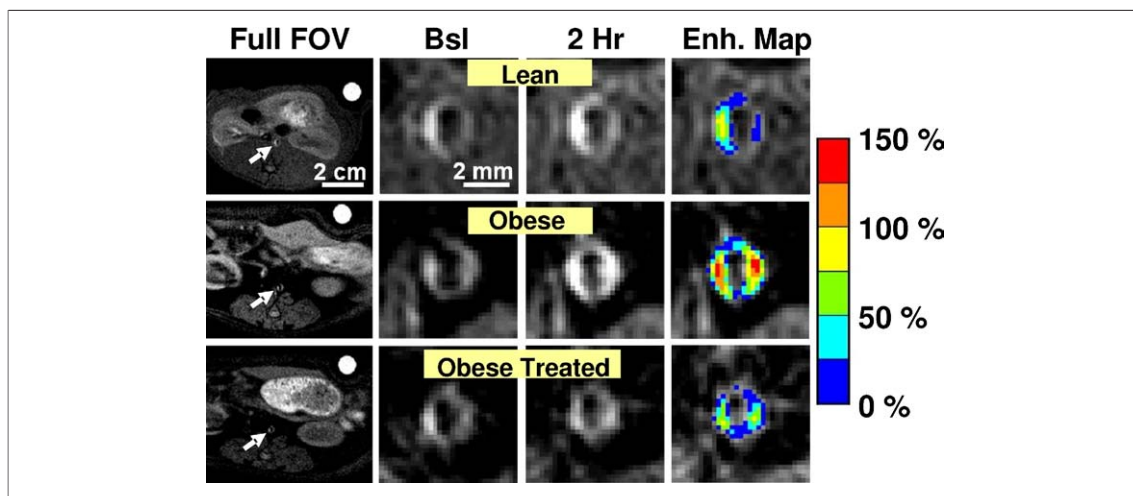
Figure 2. MR Molecular Imaging of Aortic Angiogenesis With Targeted Nanoparticles

Full field of view (FOV) of T1 weighted, fat suppressed magnetic resonance (MR) images show large abdominal fat deposits in the obese **(middle row)** and obese treated **(bottom row)** rats that were absent in the lean **(top row)** animals **(arrows** denote aortas). Magnified views of the abdominal aorta in lean, obese, and obese-treated rats at baseline (Bsl) and 2-h (2 Hr) post-injection of targeted nanoparticles show signal enhancement in the aorta wall. The percentage of signal enhancement maps (Enh. Map; false colored from **blue** to **red**) demonstrate higher MR signal enhancement in the untreated obese animal, indicating active angiogenesis supporting development of atherosclerotic lesions.

including the entire vessel circumference and all imaged slices and not only subjectively selected areas identified as "hot spots" of plaque development.

Neovascularization is a prominent feature of human atherosclerotic lesions characterized as unstable lipid-rich plaques, but only a minor component of stable fibrocalcific lesions (6). Angiogenesis

Figure 3. Serial Monitoring of Angiogenesis in the Abdominal Aorta With MR Molecular Imaging

Serial monitoring of angiogenesis in the abdominal aorta with targeted nanoparticles in the lean **(green)**, obese **(pink)**, and obese treated **(yellow)** animals. In the untreated obese animals, the MR enhancement measured 2 h post-injection steadily increases over the course of the study, indicating progressive development of angiogenesis. Neovascular enhancement in the lean and obese treated animals remained constant and low throughout the study, reflecting the reduced progression of aortic disease with benfluorex treatment. *p < 0.05. Abbreviation as in Figure 2.

not only provides a portal of entry for blood-borne cells and nutrients into the inflamed tissue (23), but these fragile neovessels are also prone to shear-induced disruption, resulting in intraplaque hemorrhage. Intraplaque hemorrhage induces amplification of intramural inflammatory and immune processes, which may ultimately progress to plaque rupture (8,24,25).

The $\alpha_v\beta_3$-integrin is a heterodimeric transmembrane glycoprotein and biomarker that is differentially up-regulated in proliferating versus quiescent endothelial cells, but it is also expressed by numerous cell types prominently represented in atherosclerotic plaques, including endothelial cells (26,27), macrophages (28), platelets (29), lymphocytes (29), and smooth muscle cells (30). We have shown that $\alpha_v\beta_3$-targeted paramagnetic nanoparticles specifically detect and quantify angiogenesis in atherosclerotic plaques of hypercholesterolemic rabbits (31). Microvessel counts have been closely correlated with the MR imaging signal enhancement, which increased monotonically at higher adventitial microvessel counts and decreased rapidly as neovessel counts decreased (32). Moreover, MR signal enhancement has been clearly shown to reflect a neovascular response to targeted antiangiogenic treatment given alone and in synergistic combination with atorvastatin therapy (32,33). Histological staining of the $\alpha_v\beta_3$-integrin itself was not performed in this study because numerous cell
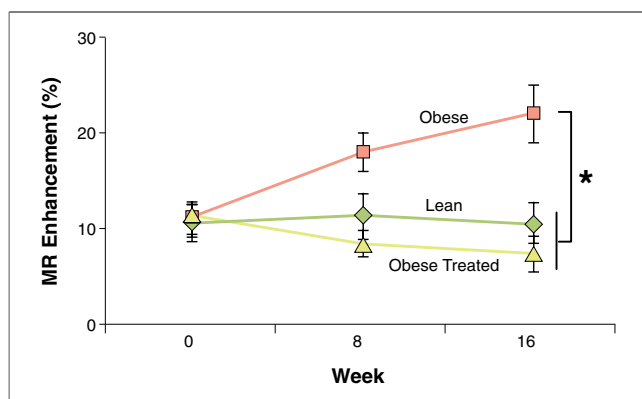
types, including macrophages, platelets, lymphocytes, and smooth muscle cells (32), express this integrin. Earlier publications have demonstrated that $\alpha_\nu\beta_3$-targeted nanoparticles are confined to the vasculature (12,32) where they can only interact with endothelial cells. Therefore, histological staining of an endothelial marker, such as von Willebrand factor, is more likely to reflect possible sites of nanoparticle binding than staining for the integrin itself, which would greatly overestimate particle binding.

Dietary benfluorex, which increases neurotransmitter serotonin levels to produce satiety and loss of appetite, decreased diet intake to the lean control consumption. Body weight and circulating levels of insulin and leptin were reduced relative to the untreated obese animals, but were still elevated compared with the lean controls, in agreement with previous reports (18,19). In earlier studies, the pairing of obese rat food intake to control animals and the feeding of benfluorex or *d*-fenfluramine have been found to diminish cardiovascular disease and myocardial lesions in this corpulent rat model (14,18,19,34,35). Ad libitum feed consumption in benfluorex-treated obese rats was comparable to the intake of their lean control counterparts, which was mirrored by a low aortic neovascular MR signal in both groups of animals. Collectively, these findings support the contention that the progression of cardiovascular disease is correlated with increasing intramural angiogenesis, which can be noninva-
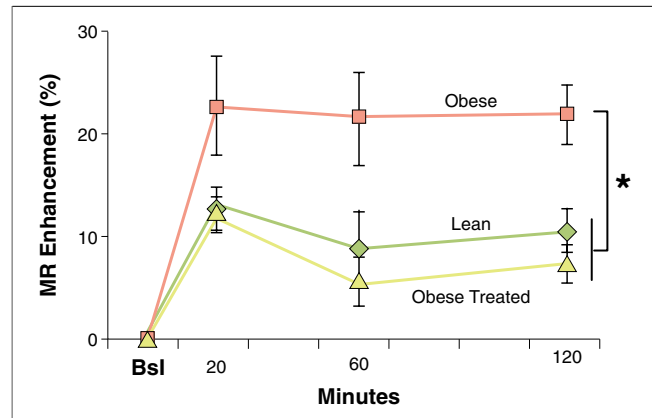

Figure 4. MR Signal Enhancement in the Aortic Wall

Signal enhancement in the aortic wall before (baseline [Bsl]) and 20, 60, and 120 min post-injection of targeted paramagnetic nanoparticles in the lean (**green**), obese (**pink**), and obese treated (**yellow**) animals at 16 weeks of the study. Neovascular contrast in the untreated obese rats increased markedly at 20 min compared with the lean or benfluorex-treated animals and remained unchanged over the remaining 100 min of scanning. *p < 0.05. Abbreviation as in Figure 2.

sively and serially interrogated and quantified with MR molecular imaging. Other changes in body weight and hormonal profiles of the obese rats were directionally similar to the appetite suppression effects of benfluorex, but only noninvasive MR assessments of angiogenesis closely paralleled the diminished food consumption effect of the lean control group.
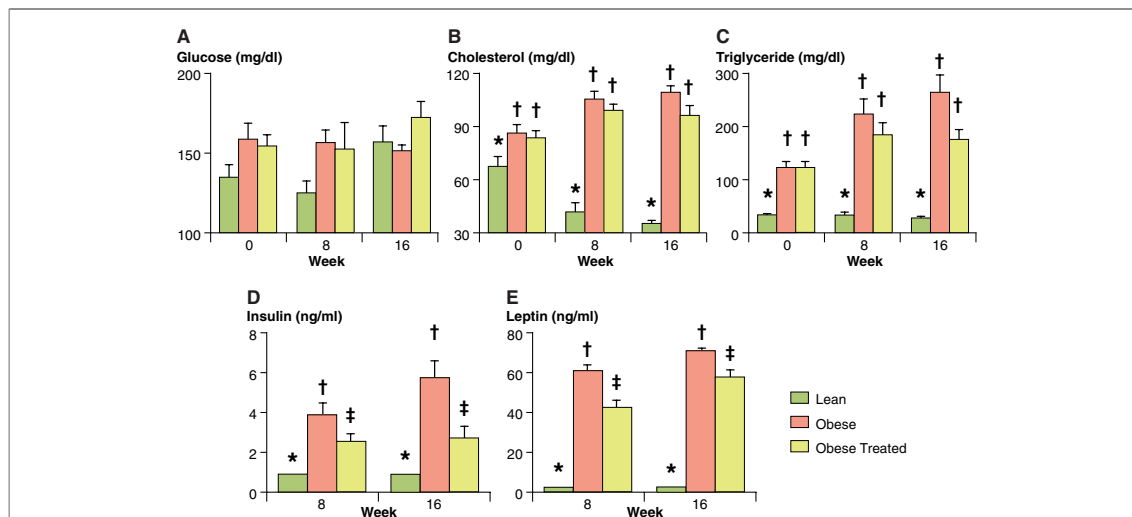

Figure 5. Fasting Blood Glucose, Cholesterol, Triglyceride, Insulin, and Leptin Levels

Fasting blood glucose (**A**), cholesterol (**B**), triglyceride (**C**), insulin (**D**), and leptin (**E**) levels in lean (**green**), obese (**pink**), and obese treated (**yellow**) animals. Glucose levels were identical for the 3 groups throughout the study. Cholesterol and triglyceride concentrations were lower in lean rats compared with the obese animals and were not significantly affected by benfluorex treatment. Insulin and leptin were markedly higher in the obese than in lean animals. Benfluorex lowered insulin and leptin levels in the obese treated rats, but not to the level in lean animals. Groups with different superscripts (*, †, ‡) within a time point are different (p < 0.05).
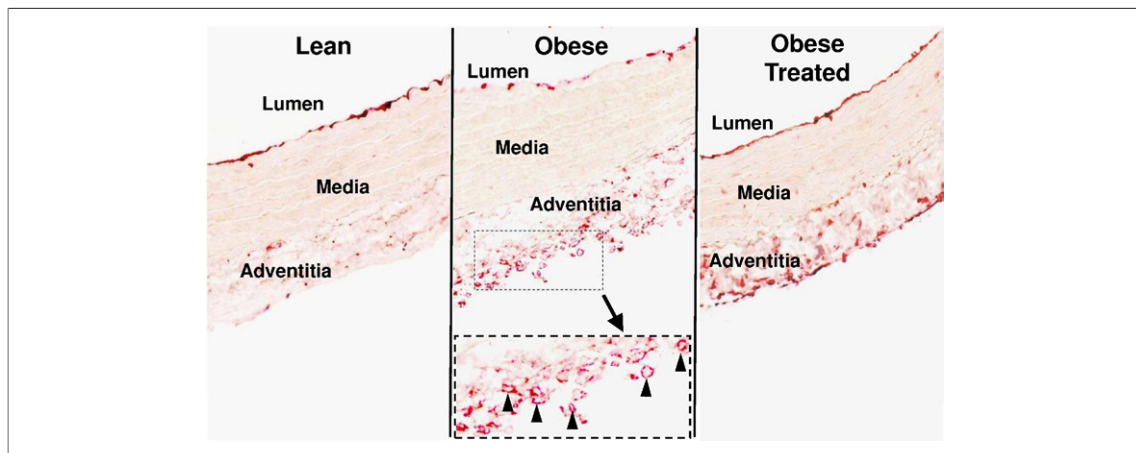
Figure 6. Increased Microvascular Density in Obese Rats

Staining of von Willebrand factor in abdominal aorta sections (×10) from lean (**left**), obese (**middle**), and obese treated (**right**) animals identifies endothelial cells in the lumen, media, and adventitia. Higher magnification inset of the untreated obese rat shows high density of small blood vessels (**arrowheads**) located in the adventitia.

Study limitations. One limitation of the present study and other animal model studies is the focus on very early atherosclerotic disease because many of the key features of human atherosclerotic plaque reported to amplify neovascular response, such as intraplaque hemorrhage and associated T cell–mediated immune response, are not present.

Figure 7. Benfluorex Normalizes Adventitial Microvascular Density

Adventitial microvessel density (microvessels/100 μm^2) in the lean (**green**), obese (**pink**), and obese treated (**yellow**) animals. Far fewer small vessels were found in both the lean and obese treated groups compared with untreated obese animals (*$p < 0.05$), corroborating the results obtained from magnetic resonance molecular imaging with $\alpha_v\beta_3$-integrin targeted nanoparticles.

Although the ameliorative effect of benfluorex on dietary intake, body weight increase, and aortic neovascular expansion in early plaque was evident, the regression or stabilization of advanced plaque remains to be demonstrated.

This study measured the MR imaging enhancement arising from only the $\alpha_v\beta_3$-integrin targeted nanoparticle formulation. Although we did not use nontargeted nanoparticles to determine the nonspecific accumulation of the contrast agent due to the hyperpermeability of angiogenic vessels, this issue has been explored in previous studies of animal models of cardiovascular disease and cancer (10,31,33). Typically, the nontargeted formulation produces approximately 50% less image enhancement compared with the targeted particles. Although it is reasonable to assume that the nontargeted agent would also yield 50% less enhancement in the JCR rat, further studies will be required to assess the nonspecific contribution and the dependence of particle dose and post-injection time point on the nontargeted component.

The clinical use of benfluorex has been discontinued in the U.S. due to safety concerns. However, the molecular imaging techniques described in this study are sensitive to neovascular proliferation in the aortic wall and are not limited to only detecting the response to benfluorex treatment. This method could be applied to monitoring the end-organ effects of a vast array of therapeutic approaches, such as lifestyle modifications, surgical interventions, lipid-lowering medications, and glucose normalization.
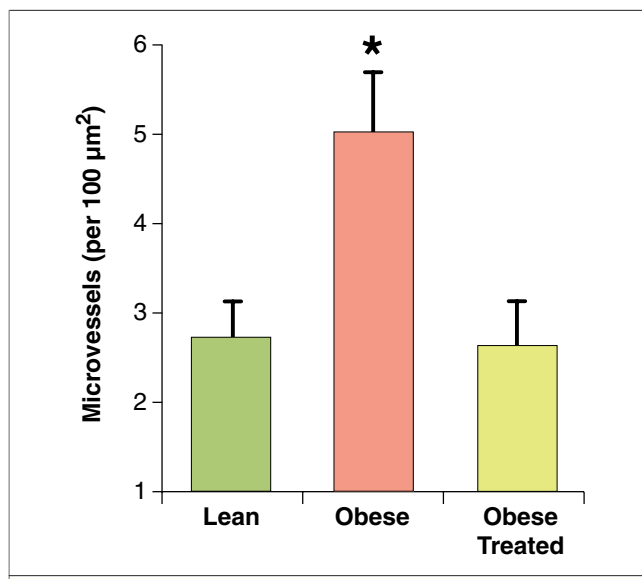
CONCLUSIONS

These data represent the first report of molecular imaging of angiogenesis at a clinical field strength to detect early metabolic vasculopathy and to quantify therapeutic response to benfluorex in the corpulent JCR:LA-cp rat model of metabolic syndrome. Benfluorex, an appetite suppressant, reduced ad libitum food intake equivalent to that in lean control rats, which reduced body weight, insulin, and leptin levels of the obese rats relative to those of untreated animals. However, none of these measures were reduced to the control level in the lean rats. MR neovascular signal enhancement, on the other hand, was markedly reduced by benfluorex to the contrast levels measured in the lean rats, which closely paralleled the appetite suppression effects. These results support the contention that MR molecular imaging of angiogenesis with integrin-targeted nanoparticles could provide a sensitive, high-resolution signal for monitoring progression and treatment of cardiovascular disease.

REFERENCES

1. Koenig W, Sund M, Frohlich M, et al. C-reactive protein, a sensitive marker of inflammation, predicts future risk of coronary heart disease in initially healthy middle-aged men: results from the MONICA (Monitoring Trends and Determinants in Cardiovascular Disease) Augsburg Cohort Study, 1984 to 1992. Circulation 1999; 99:237–42.

2. Ridker PM, Buring JE, Cook NR, Rifai N. C-reactive protein, the metabolic syndrome, and risk of incident cardiovascular events: an 8-year follow-up of 14 719 initially healthy American women. Circulation 2003; 107:391–7.

3. Ridker PM, Rifai N, Rose L, Buring JE, Cook NR. Comparison of C-reactive protein and low-density lipoprotein cholesterol levels in the prediction of first cardiovascular events. N Engl J Med 2002;347:1557–65.

4. de Boer OJ, van der Wal AC, Teeling P, Becker AE. Leucocyte recruitment in rupture prone regions of lipid-rich plaques: a prominent role for neovascularization? Cardiovasc Res 1999;41: 443–9.

5. Kolodgie FD, Virmani R, Burke AP, et al. Pathologic assessment of the vulnerable human coronary plaque. Heart 2004;90:1385–91.

6. Moreno PR, Purushothaman KR, Fuster V, et al. Plaque neovascularization is increased in ruptured atherosclerotic lesions of human aorta: implications for plaque vulnerability. Circulation 2004;110:2032–8.

7. Virmani R, Burke AP, Kolodgie FD, Farb A. Pathology of the thin-cap fibroatheroma: a type of vulnerable plaque. J Interv Cardiol 2003;16:267–72.

8. Virmani R, Kolodgie FD, Burke AP, et al. Atherosclerotic plaque progression and vulnerability to rupture: angiogenesis as a source of intraplaque hemorrhage. Arterioscler Thromb Vasc Biol 2005;25:2054–61.

9. Schmieder AH, Winter PM, Caruthers SD, et al. Molecular MR imaging of melanoma angiogenesis with alphanubeta3-targeted paramagnetic nanoparticles. Magn Reson Med 2005;53:621–7.

10. Winter PM, Caruthers SD, Kassner A, et al. Molecular imaging of angiogenesis in nascent Vx-2 rabbit tumors using a novel alpha(nu)beta3-targeted nanoparticle and 1.5 tesla magnetic resonance imaging. Cancer Res 2003; 63:5838–43.

11. Winter PM, Caruthers SD, Yu X, et al. Improved molecular imaging contrast agent for detection of human thrombus. Magn Reson Med 2003; 50:411–6.

12. Winter PM, Schmieder AH, Caruthers SD, et al. Minute dosages of alpha(nu)beta3-targeted fumagillin nanoparticles impair Vx-2 tumor angiogenesis and development in rabbits. FASEB J 2008;22:2758–67.

13. Russell JC, Graham SE, Dolphin PJ. Glucose tolerance and insulin resistance in the JCR:LA-corpulent rat: effect of miglitol (Bay m1099). Metabolism 1999;48:701–6.

14. Russell JC, Graham SE, Richardson M. Cardiovascular disease in the JCR:LA-cp rat. Mol Cell Biochem 1998; 188:113–26.

15. Russell JC, Koeslag DG, Amy RM, Dolphin PJ. Plasma lipid secretion and clearance in hyperlipidemic JCR:LA-corpulent rats. Arteriosclerosis 1989;9:869–76.

16. Russell JC, Koeslag DG, Amy RM, Dolphin PJ. Independence of myocardial disease in the JCR:LA-corpulent rat on plasma cholesterol concentration. Clin Invest Med 1991; 14:288–95.

17. Brindley DN, Hales P, al-Sieni AI, Russell JC. Decreased serum lipids, serum insulin and triacylglycerol synthesis in adipose tissue of JCR:LA-corpulent rats treated with benfluorex. Biochim Biophys Acta 1991;1085: 119–25.

18. Russell JC, Graham SE, Dolphin PJ, Amy RM, Wood GO, Brindley DN. Antiatherogenic effects of long-term benfluorex treatment in male insulin resistant JCR:LA-cp rats. Atherosclerosis 1997;132:187–97.

19. Russell JC, Graham SE, Dolphin PJ, Brindley DN. Effects of benfluorex on serum triacylglycerols and insulin sensitivity in the corpulent rat. Can J Physiol Pharmacol 1996;74: 879–86.

20. Meoli DF, Sadeghi MM, Krassilnikova S, et al. Noninvasive imaging of myocardial angiogenesis following experimental myocardial infarction. J Clin Invest 2004;113:1684–91.

21. Sadeghi MM, Krassilnikova S, Zhang J, et al. Detection of injury-induced vascular remodeling by targeting activated alphavbeta3 integrin in vivo. Circulation 2004;110:84–90.

22. Neubauer AM, Sim H, Winter PM, et al. Nanoparticle pharmacokinetic profiling in vivo using magnetic resonance imaging. Magn Reson Med 2008;60:1353–61.

23. Moreno PR, Purushothaman KR, Sirol M, Levy AP, Fuster V. Neovascularization in human atherosclerosis. Circulation 2006;113:2245–52.

24. Kolodgie FD, Gold HK, Burke AP, et al. Intraplaque hemorrhage and progression of coronary atheroma. N Engl J Med 2003;349:2316–25.

25. Kolodgie FD, Narula J, Yuan C, Burke AP, Finn AV, Virmani R. Elimination of neoangiogenesis for plaque stabilization: is there a role for local drug therapy? J Am Coll Cardiol 2007;49:2093–101.

26. Cheresh DA. Integrins in thrombosis, wound healing and cancer. Biochem Soc Trans 1991;19:835–8.

27. Friedlander M, Theesfeld CL, Sugita M, et al. Involvement of integrins alpha v beta 3 and alpha v beta 5 in ocular neovascular diseases. Proc Natl Acad Sci U S A 1996;93:9764–9.

28. De Nichilo MO, Burns GF. Granulocyte-macrophage and macrophage colony-stimulating factors differentially regulate alpha v integrin expression on cultured human macrophages. Proc Natl Acad Sci U S A 1993;90: 2517–21.

29. Helluin O, Chan C, Vilaire G, Mousa S, DeGrado WF, Bennett JS. The activation state of alphavbeta 3 regulates platelet and lymphocyte adhesion to intact and thrombin-cleaved osteopontin. J Biol Chem 2000;275: 18337–43.

30. Itoh H, Nelson PR, Mureebe L, Horowitz A, Kent KC. The role of integrins in saphenous vein vascular smooth muscle cell migration. J Vasc Surg 1997;25:1061–9.

31. Winter PM, Morawski AM, Caruthers SD, et al. Molecular imaging of angiogenesis in early-stage atherosclerosis with alpha(v)beta3-integrin-targeted nanoparticles. Circulation 2003;108:2270–4.

32. Winter PM, Caruthers SD, Zhang H, Williams TA, Wickline SA, Lanza GM. Antiangiogenic synergism of integrin-targeted fumagillin nanoparticles and atorvastatin in atherosclerosis. J Am Coll Cardiol Img 2008;1: 624–34.

33. Winter PM, Neubauer AM, Caruthers SD, et al. Endothelial alpha (v)beta3 integrin-targeted fumagillin nanoparticles inhibit angiogenesis in atherosclerosis. Arterioscler Thromb Vasc Biol 2006;26:2103–9.

34. Russell JC, Dolphin PJ, Graham SE, Amy RM, Brindley DN. Improvement of insulin sensitivity and cardiovascular outcomes in the JCR:LA-cp rat by D-fenfluramine. Diabetologia 1998;41:380–9.

35. Russell JC, Proctor SD, Kelly SE, Brindley DN. Pair feeding-mediated changes in metabolism: stress response and pathophysiology in insulin-resistant, atherosclerosis-prone JCR: LA-cp rats. Am J Physiol Endocrinol Metab 2008;294:E1078–87.

Key Words: angiogenesis ■ atherosclerosis ■ metabolic syndrome ■ nanoparticle.